Clays and Clay Minerals, Vol. 67, No. 6:471–480, 2019

BENTONITE/MAGNETITE COMPOSITE FOR REMOVAL OF NITROFURAZONE

Olga V. Alekseeva[1], Anna N. Rodionova[1], Andrew V. Noskov[1] *, and Alexander V. Agafonov[1]

[1]G.A. Krestov Institute of Solution Chemistry, Russian Academy of Sciences, Akademicheskaya str., 1, Ivanovo 153045, Russia

Abstract—The presence of pharmaceutical pollutants in the environment is one of the most pressing environmental problems. Adsorption from solution is an effective way to remove pharmaceuticals from liquid media, but the problem then is to separate the adsorbent from the liquids. The objective of the present study was to remove nitrofurazone from aqueous solutions using a bentonite/magnetite composite, prepared by co-precipitation of magnetite with bentonite, which could then be collected by magnetic separation. The bentonite/magnetite composite was characterized using diverse techniques, such as X-ray diffraction, scanning electron microscopy, low-temperature N_2 adsorption/desorption, laser diffraction, and magnetization measurements. The particle size of the composite material did not exceed 50 μm and the particle size distribution was mono-modal with a maximum at 3.2 μm. The strong hysteresis in the magnetization curve revealed that the bentonite/magnetite particles were ferromagnetic. Adsorption of nitrofurazone by the bentonite/magnetite composite from aqueous solutions was measured and the amount of nitrofurazone adsorbed was 3.2×10^{-2} mmol/g. The adsorption kinetics of nitrofurazone to the bentonite/magnetite composite followed a pseudo-second-order kinetics equation. Upon adsorption, hydrogen bonds were formed between the amide groups of nitrofurazone and oxygen groups in bentonite.

Keywords—Adsorption · Bentonite/magnetite Composites · IR spectroscopy · Magnetic Properties · Nitrofurazone · X-ray diffraction

INTRODUCTION

Recently, increasing attention has been paid to the development of multifunctional materials consisting of layered aluminosilicates for use in biotechnology, medicine, and ecology (Alekseeva et al. 2017, 2019; Lin et al. 2017; Martinez-Costa et al. 2018; Sahnoun et al. 2018; Abidi et al. 2019). Of the entire variety of aluminosilicates, bentonite clay minerals occur widely in nature and are most promising for the production of composites (Gil et al. 2008; Bee et al. 2018).

Bentonite consists primarily (near 80%) of montmorillonite (Mnt), which is a natural 2:1 type clay mineral. Other components of bentonite are illite, calcite, plagioclase, muscovite, etc. This clay mineral exhibits anisotropy, a regular distribution of meso- and micropores, thermal stability, and the presence of various reactive centers. As a low-cost and readily available mineral with many excellent properties, bentonite has been applied in the fields of catalysis, separation, biology, medicine, adsorption, sensor environmental control, etc. (Park et al. 2009; Ruiz-Hitzky et al. 2010; Lee et al. 2011; Zhou et al. 2011; Datta 2013; Yu et al. 2013; Deng et al. 2017; Gamba et al. 2017).

Clay minerals are natural adsorbents and are known for their hydrophilic nature. Due to the presence of exchangeable cations in their structure, large specific surface area, swelling properties, as well as their wide availability, some of the most common types of clay minerals such as kaolinite and montmorillonite (the most prevalent clay mineral in bentonite) have already been tested for the removal of a variety of organic pollutants (Jaynes & Boyd 1991; Zhang et al. 2010; Dordio et al. 2017).

Bentonite can be modified to improve its sorption ability. One modification is coating with metal particles (Golubeva 2016). The introduction of such nanoparticles promotes destruction of the hierarchical structure formed because of the coalescence of individual crystallites and can cause changes in the texture and physicochemical properties of the resulting composite. Of the metal compounds used, iron oxides, e.g. magnetite Fe_3O_4, which is characterized by a positive magnetic susceptibility, are of interest (Barraqué et al. 2018). This property is used to make magnetically controlled adsorbents, which results in intensification of the solid–liquid separation process (Pastukhov et al. 2013). The use of magnetic clay as an adsorbent to remove hazardous and toxic substances from aqueous media is extremely important. Among different sources of water contamination, pollution by different types of drugs has become a major concern. Moreover, even residual amounts of such substances in pharmaceutical wastewater have a negative impact on human health and the ecological balance of the environment.

Many pharmaceutical wastewaters contain nitrofurans, i.e. antibacterial drugs used widely in medicine (Biosic et al. 2017; Grenni et al. 2018). Nitrofurans are synthetic therapeutic drugs with a broad antiseptic effect against bacteria, mold, yeast, and viruses. One of the representatives of the nitrofuran group is nitrofurazone which is used widely in surgical practice in the form of ointments and water and alcohol solutions.

Few studies of nitrofuran sorption are found in the literature and certain aspects of adsorption phenomena on the surface of clay minerals have not been studied sufficiently well. Further research of this process is needed to enhance its effectiveness.

* E-mail address of corresponding author: avn@isc-ras.ru
DOI: 10.1007/s42860-019-00037-w

The aim of the present study was, therefore, to make a bentonite/magnetite composite; to investigate its structure, morphology, and physicochemical properties; and to explore the possibility of using the composite for the removal of nitrofurazone from water solutions.

MATERIALS AND METHODS

Materials

Bentonite, ferric chloride hexahydrate ($FeCl_3 \cdot 6H_2O$), ferrous sulfate heptahydrate ($FeSO_4 \cdot 7H_2O$), and aqueous ammonia (NH_4OH) were supplied by Sigma Aldrich, St. Louis, Missouri, USA. The materials listed were used for synthesis of a bentonite/magnetite powder. Nitrofurazone (furacilin, 5-nitro-2-furfural semicarbazone) was used to study adsorption activity of the bentonite/magnetite composite.

All reagents were of analytical reagent grade; doubly distilled water was used for the preparation of solutions.

Synthesis of Bentonite/magnetite Composites

Bentonite/magnetite powder was produced by co-precipitation of iron salts into clay. For this purpose 11.8 g of $FeCl_3 \cdot 6H_2O$ and 6.25 g of $FeSO_4 \cdot 7H_2O$ were dissolved in water (250 mL). Then dried bentonite (15 g) was dispersed in this solution by intensive stirring and ultrasonic vibration at 60°C for 10 min. For this, a Grad 13-35 (Grad-Technology, Moscow, Russia) ultrasonic bath was used at 205 W. The resultant suspension was stirred using a magnetic stirrer (600 rpm) at 80°C for 1 h.

For the precipitation of magnetite particles onto the surface and in pores of the bentonite, aqueous ammonia (25%) was added dropwise to the mixture to raise the pH to 11.0 while maintaining vigorous stirring. The reaction proceeded according to the following scheme:

$$FeSO_4 \cdot 7H_2O + 2FeCl_3 \cdot 6H_2O + 8NH_3 \cdot H_2O \rightarrow Fe_3O_4\downarrow + 6NH_4Cl + (NH_4)_2SO_4 + 23H_2O$$

The resulting suspension turned black, indicating the formation of magnetite. The resulting suspension was left for 24 h. The final product was then washed thoroughly with distilled water until a pH of ~7 was reached. Then it was centrifuged (CM-6M centrifuge (ELMI, Riga, Latvia), 2300 ×*g*) and dried at 60°C.

Pure magnetite was also obtained by mixing the corresponding reagents and following the same procedure described previously without the clay mineral.

Characterization

Granulometric analysis of the bentonite/magnetite powder was performed using an Analysette 22 COMPACT (Idar-Oberstein, Germany) particle size analyzer.

The surface morphology and composition of magnetized clay samples were investigated using a Tescan Vega 3 SBH (Brno, Czech Republic) scanning electron microscope equipped with an energy-dispersive X-ray spectroscopy (EDS) detector.

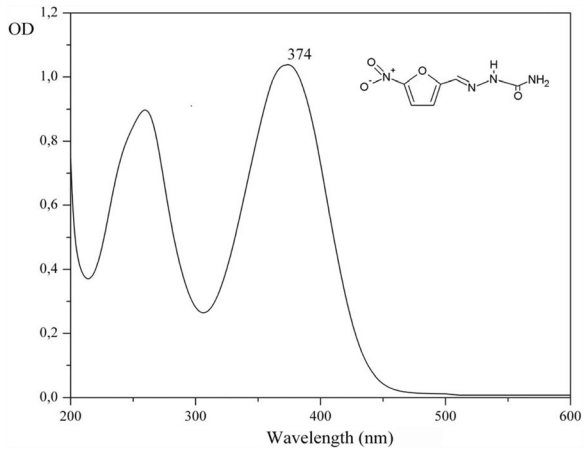

Fig. 1 UV/Vis spectrum of nitrofurazone and its chemical structure

The porosity parameters were determined using the method of low-temperature (77 K) nitrogen vapor adsorption-desorption with the use of a NOVAtouch NT LX-1 (Quantachrome, Boynton Beach, Florida, USA) surface area analyzer. Before the adsorption measurements, the sample powders were kept in a vacuum drying oven at a temperature of 100°C for 7 h. Analysis of isotherms was performed using the Brunauer-Emmett-Teller (BET) and Barrett-Joyner-Halenda (BJH) models.

The structure of the powders was investigated by means of X-ray diffraction (XRD) in the angle range of 2–70°2θ using a DRON-UM1 (St. Petersburg, Russia) diffractometer (CuKα radiation, λ = 0.154 nm), operating at a voltage of 40 kV and a current of 40 mA.

Infrared (IR) transmission spectra of bentonite/magnetite powders were registered using an Avatar 360 FT-IR ESP Fourier-transform spectrometer (Thermo Nicolet, Woodland, California, USA) within a wavenumber range of ~4000–400 cm^{-1} with 16

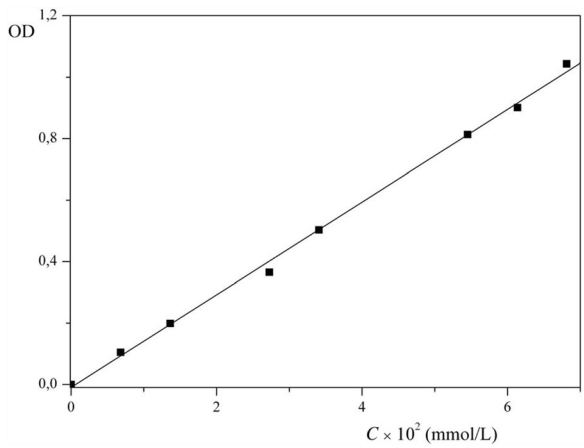

Fig. 2 Calibration dependence 'absorbance versus concentration' for nitrofurazone solution

https://doi.org/10.1007/s42860-019-00037-w Published online by Cambridge University Press

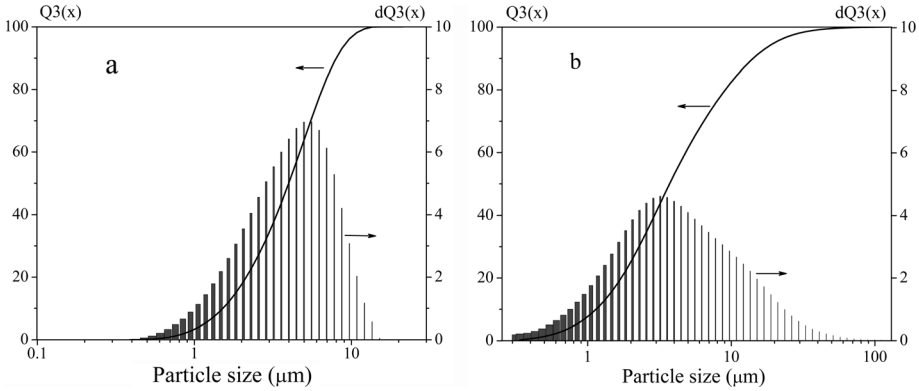

Fig. 3 Cumulative and differential particle-size distributions for (**a**) bentonite and (**b**) magnetic bentonite/magnetite composite

scans at a resolution of 0.9 cm^{-1}. For measurements, the samples were pressed into KBr pellets at a mass ratio of 1:100.

The magnetic property was measured using a vibrating sample magnetometer at room temperature up to a maximum magnetic field of 4000 Oe.

Adsorption Experiments

The adsorption behavior of the bentonite/magnetite powder was studied at ambient temperature to measure the distribution of nitrofurazone in the heterogeneous adsorbent/(aqueous nitrofurazone) system. For this purpose, aqueous solutions of nitrofurazone at various concentrations were prepared by dissolving nitrofurazone in 0.9% sodium chloride solution (pH = 5.5). The choice of pH was due to poor solubility of nitrofurazone in water and its good solubility in an acidic medium.

Then, a weighed portion of the adsorbent (m = 0.005 g) was placed into 25 mL glass tubes, mixed with 5 mL (V) of aqueous nitrofurazone, stirred for a certain time interval (from 4 to 362 min), and then the phases were separated using a centrifuge for 2 min.

In kinetics experiments, the initial nitrofurazone concentration in solution (C_0) was $6.813 \cdot 10^{-2}$ mmol/L. The concentration of nitrofurazone in solution after adsorption (C_t) was determined using a UV-Vis spectrophotometer (T70+UV/Vis, PG Instrument Co Ltd., Lutterworth, UK) at 374 nm (Fig. 1). For this purpose, the pre-calibration dependence of absorbance on the concentration of nitrofurazone solution was plotted in the concentration range of (~0–7)×10^{-2} mmol/L. The calibration curve was highly reproducible and linear (Fig. 2).

All the experimental data reported from the batch adsorption experiments were the average values of three tests (error <±5%).

The amount of adsorbed drug (A_t) was calculated as follows:

$$A_t = \frac{(C_0 - C_t)V}{m} \quad (1)$$

Then the A_t value was plotted against time (t).

The adsorption kinetics data for the adsorbent/nitrofurazone system were analyzed by non-linear fitting of two models: pseudo-first-order (model I) and pseudo-second-order (model II) (Ho 2004; Cazetta et al. 2011), according to Eqs. 2 and 3:

$$A_t = A_{eq}\left[1 - e^{-k_1 t}\right] \quad (2)$$

$$A_t = A_{eq}\frac{k_2 A_{eq} t}{1 + k_2 A_{eq} t} \quad (3)$$

where A_{eq} is the equilibrium concentration of adsorbed nitrofurazone; k_1 and k_2 are the rate constants.

The A_{eq}, k_1, and k_2 values were determined on the basis of the experimental data using non-linear curve fitting (*OriginPro7.0* software package). The adequacy of the model was evaluated by the coefficient of determination (R^2) and the reduced adequacy parameter (χ^2_{red}) determined as follows:

$$\chi^2_{red} = \frac{\sum_{i=1}^{n}\left[y_i - f(x_i, p_1, p_2)\right]^2}{n-2} \quad (4)$$

where y_i represents the A_t values found experimentally; $f(x_i, p_1, p_2)$ is the fitting function; n is the total number of experimental points used in the fitting; and p_i values are the fitting parameters.

The adsorption isotherms of nitrofurazone on bentonite/magnetite were determined when the initial concentration of adsorbate in solution was in the range ((~0.512–5.09) 0.512~5.09)×10^{-2} mmol/L. The equilibrium amount of

Table 1 Particle-size distributions for the bentonite and bentonite/magnetite composite

Material	Mode (μm)	Average size (μm)	Sizes relating to percentiles (μm)		
			10%	50%	90%
Bentonite	5.6	4.5	1.5	4.0	7.9
Bentonite/magnetite	3.2	6.3	1.1	3.7	14.0

https://doi.org/10.1007/s42860-019-00037-w Published online by Cambridge University Press

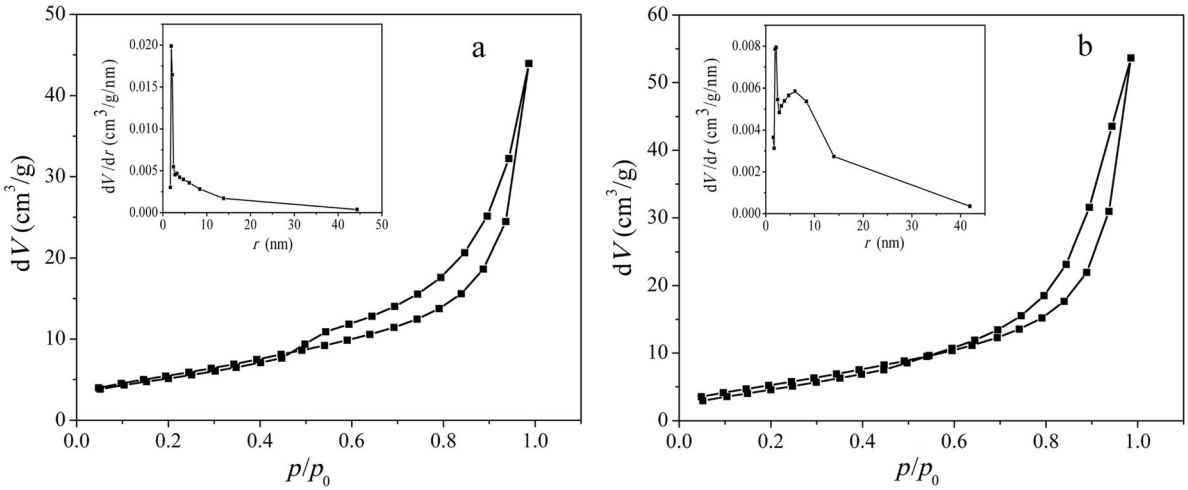

Fig. 4 Isotherms of low-temperature nitrogen adsorption-desorption and BJH pore-size distribution for (**a**) bentonite and (**b**) magnetic bentonite/magnetite composite

nitrofurazone in the adsorbent phase (A_{eq}) was plotted against the equilibrium drug concentration in solution (C_{eq}) and fitted using the Langmuir, Freundlich, and Temkin isotherms as mathematical fitting models, given by Eqs. 5, 6, and 7, respectively:

$$A_{eq} = A_m \frac{K_L C_{eq}}{1 + K_L C_{eq}} \quad (5)$$

$$A_{eq} = K_F (C_{eq})^{1/n} \quad (6)$$

$$A_{eq} = B_T ln[K_T C_{eq}], \quad (7)$$

where A_m is the theoretical maximum monolayer adsorption capacity; K_L is the Langmuir constant; K_F is the Freundlich constant; $1/n$ is a heterogeneity factor which ranges from 0 to 1; and B_T and K_T are the Temkin isotherm constants.

The Langmuir model is based on the supposition of monolayer adsorption on a structurally homogenous adsorbent, where all sorption sites are identical and energy equivalent. The Freundlich equation is applicable to adsorption on heterogeneous surfaces with a non-uniform distribution of heat of adsorption. The Temkin isotherm model assumes that adsorption is characterized by the uniform distribution of binding energies.

RESULTS AND DISCUSSION

Granulometric Composition

Granulometric analysis of bentonite and bentonite/magnetite powders revealed that these materials contained particles which were predominantly <50 μm in diameter (Fig. 3(a,b)). The average particle size, the peak in the particle-size distribution (mode), and the sizes corresponding to 10%, 50%, and 90% of the overall particle population were determined (Table 1). For both bentonite and bentonite/magnetite powders, the particle-size distributions were mono-modal with peaks at 5.6 and 3.2 μm, respectively.

Porous Structure

To estimate the structural and adsorption parameters for bentonite and the synthesized magnetic clay, the nitrogen adsorption–desorption method was used. The measured N_2 adsorption-desorption isotherms (Fig. 4a,b) belong to type IV according to the IUPAC classification (ALOthman 2012). When the relative pressure p/p_0 was low, adsorption was limited only by formation of the thin layer on pore walls. The p/p_0 value of 0.5 was attributed to the beginning of capillary condensation in the thinnest pores. When the relative pressure was close to 1, an abrupt rise was observed in the adsorption isotherm which indicated the presence of large pores in the material.

Analysis of the isotherms revealed the quantitative indices of pore structure for both bentonite and bentonite/magnetite powders, and that the total pore volumes were 0.07 and 0.08 cm^3/g, respectively. The specific surface areas were calculated using both the BET (S_{BET}) and BJH (S_{BJH}) models. The specific surface area from both models was greater for bentonite/magnetite than for bentonite alone (Table 2), giving S_{BET} and S_{BJH} values of 20.30 and 25.10 m^2/g, respectively, for bentonite/magnetite and 20.18 and 23.24 m^2/g, respectively, for bentonite. The differences between S_{BET} and S_{BJH} values are probably due to different assumptions inherent in the BET and BJH models. For example, unlike the BET model, the BJH model is based on the Kelvin theory of cylindrical pore filling.

Table 2 Specific surface areas and porosities of materials investigated

Parameter	Value	
	Bentonite	Bentonite/magnetite
BET Surface area (m^2/g)	20.18	20.30
BJH Surface area (m^2/g)	23.24	25.10
Total pore volume (cm^3/g)	0.07	0.08
Average pore radius (nm)	6.75	8.20

https://doi.org/10.1007/s42860-019-00037-w Published online by Cambridge University Press

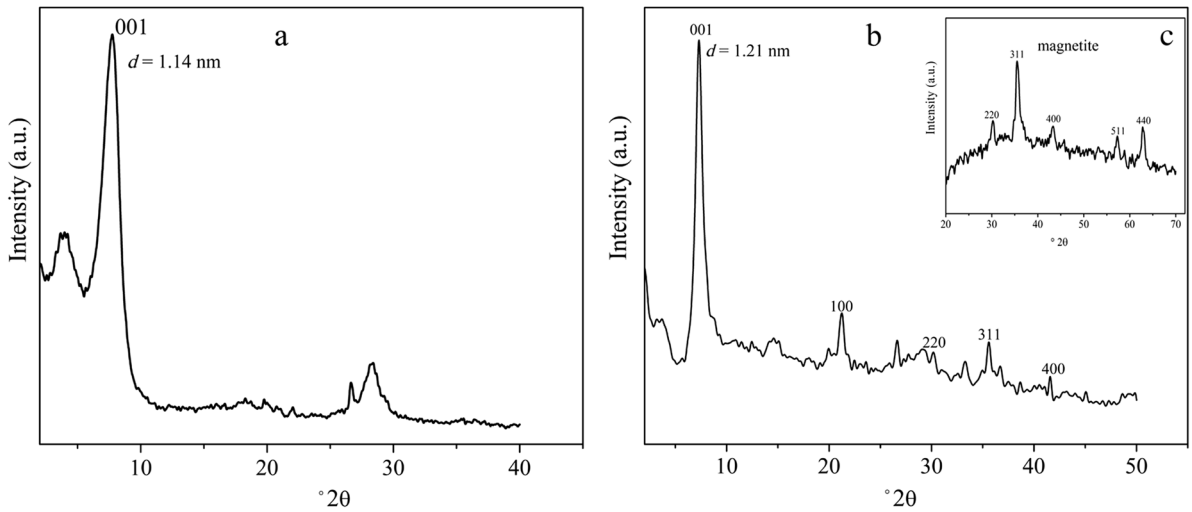

Fig. 5 XRD patterns for (**a**) bentonite, (**b**) bentonite/magnetite, and (**c**) magnetite (insert)

The pore-size distribution was plotted using the BJH model (inserts in Fig. 4a,b). The pore sizes in both bentonite and bentonite/magnetite composite were <45 nm. The pore-size distribution of bentonite/magnetite, however, was wider (with peaks near 4 and 9 nm) and the average pore radius was larger (8.20 nm vs 6.75 nm for bentonite).

Crystal Structure

The crystal structures of bentonite, magnetite, and bentonite/magnetite powders were evaluated by XRD measurements (Fig. 5). The XRD pattern of bentonite (Fig. 5a) contains a pronounced reflection at 7.76°2θ. This characteristic peak is assigned to the (001) plane, which agrees well with the reference pattern for montmorillonite (Joint Committee on Powder Diffraction Standards (JCPDS) card no. 13-0135).

In the XRD pattern of magnetite (Fig. 5c), the diffraction peaks at 30.20, 35.62, 43.24, 57.32, and 62.71°2θ confirmed the existence of the Fe_3O_4 pure phase (JCPDS card no. 65-3107). The listed peaks can be indexed (as face-centered cubic Fe_3O_4 with lattice constant a = 0.84 nm) to the crystal planes (220), (311), (400), (511), and (440), respectively.

In the XRD pattern of bentonite/magnetite (Fig. 5b), the most intense diffraction peak at 7.30°2θ was assigned to the (001) crystal plane in bentonite. The characteristic peaks corresponding to planes (220), (311), and (400) in magnetite remained and were not obviously shifted. So, the Fe_3O_4 phase was not changed in the bentonite/magnetite composite.

On the basis of the patterns obtained, the interlayer distances, d, and crystallites sizes, L, in bentonite/magnetite were calculated. For this, Bragg's law (Eq. 8) and the Scherrer equation (Eq. 9) were applied to the (001) peak:

$$2d\sin\theta_0 = n\lambda \tag{8}$$

$$L = \frac{0.94\lambda}{\beta cos\theta_0} \tag{9}$$

where λ is the X-ray wavelength (λ = 0.154 nm), n is the order of reflection, β is the full width at half maximum (radian), and θ_0 is the Bragg angle.

An experimental summary for the bentonite and bentonite/magnetite powders (Table 3) demonstrated that, with the introduction of magnetite, the basal spacing increased slightly from 1.14 to 1.21 nm. Apparently, this increase was caused by the attachment of magnetite to the edges of the clay particles. The crystallite size increased also (Table 3).

Magnetic Behavior

Magnetic materials are of scientific interest due to their adsorbent ability under external magnetic fields. The possible uses of the magnetic material depend on the size of the hysteresis loop and coercivity. Substances with a wide hysteresis loop and high coercivity are used to produce permanent magnets, while materials with a narrow hysteresis loop and low coercivity are required for the manufacture of transformer and generator cores.

The plot of magnetization (M) vs magnetic field (H) recorded for synthesized bentonite/magnetite powder showed a strong hysteresis, indicating that the resultant bentonite/magnetite particles were ferromagnetic (Fig. 6). The inset photograph shows that the composite powder dispersed in water could be separated easily, within several minutes, by an external magnetic field.

Table 3 Crystal parameters for bentonite and bentonite/magnetite powders

Powder	°2θ	β (deg)	d (nm)	L (nm)
Bentonite	7.76	1.39	1.14	5.98
Bentonite/magnetite	7.30	0.79	1.21	10.52

https://doi.org/10.1007/s42860-019-00037-w Published online by Cambridge University Press

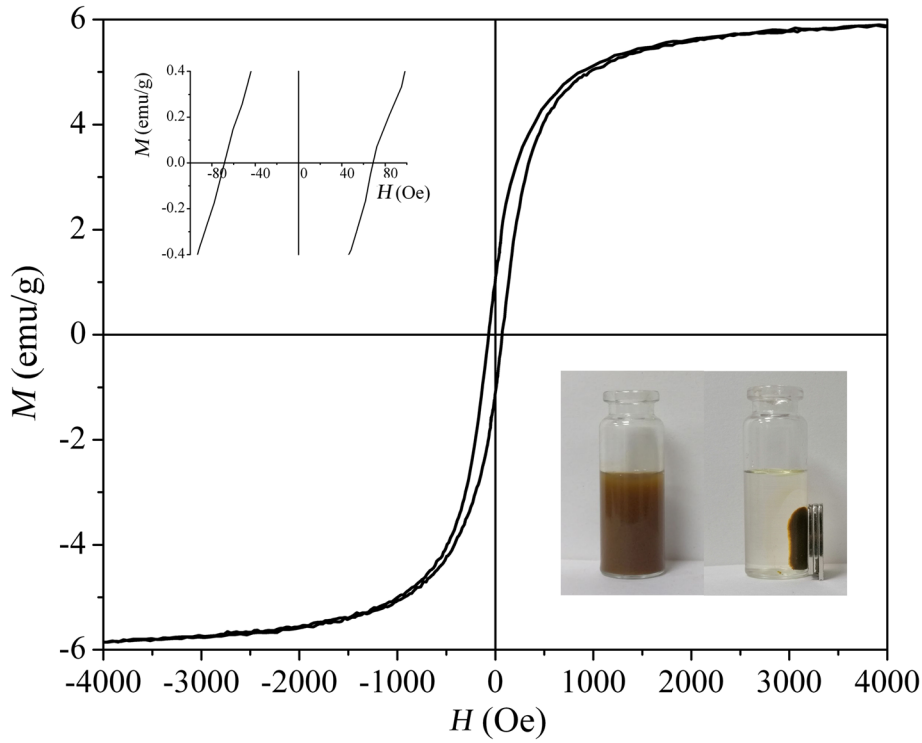

Fig. 6 Magnetization curves for bentonite/magnetite composite

On the basis of the plot of M vs H and its enlargement near the origin (other insertion in Fig. 6), the remanent magnetization (M_r), saturation magnetization (M_s), coercivity (H_c), and squareness (M_r/M_s) were determined (Table 4).

The magnetic properties of magnetite (pure) synthesized by the same chemical co-precipitation of iron salts, as bentonite/magnetite powders used in the current study, were reported by Liao & Chen (2002) (Table 4). For composite powders, the saturation magnetization was >10 times less than for pure magnetite. Apparently, the reason for this is the smaller content of the magnetic component in the composite powder. The decrease in the M_s value for composites compared to pure magnetite is consistent with the results from other studies (Liao & Chen 2002; Barraqué et al. 2018; Sebayang et al. 2018).

The value of H_c for magnetite is significantly less than that measured for the bentonite/magnetite powder in the present study. Apparently, the increase in H_c in the composite is a consequence of the change in the magnetic dipole interaction after the precipitation of the magnetite particles in the pores and among clay layers.

Table 4 Magnetic properties of bentonite/magnetite powder and pure magnetite

Powder	M_s (emu/g)	M_r (emu/g)	H_c (Oe)	M_r/M_s
Bentonite/magnetite	6.0	1.03	68.8	0.172
Magnetite *	63.2	0.83	8.5	0.013

*Values for magnetite were obtained from Liao & Chen (2002).

Adsorption of Nitrofurazone by Bentonite/Magnetite from Aqueous Media

To assess the value of bentonite/magnetite powder in environmental protection, its performance in the removal of nitrofurazone was studied.

Surface Morphology and Composition SEM-EDX analysis was carried out to evaluate the surface morphology and composition of the bentonite/magnetite powder and to confirm the adsorption of nitrofurazone on it (Figs. 7 and 8). The

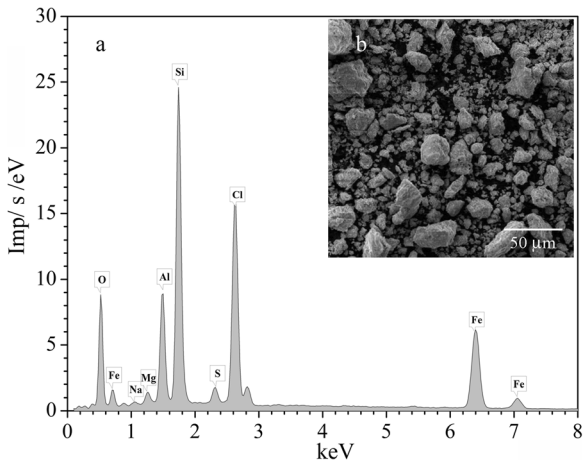

Fig. 7 EDX analysis (**a**) and SEM image (**b**) of the bentonite/magnetite composite

https://doi.org/10.1007/s42860-019-00037-w Published online by Cambridge University Press

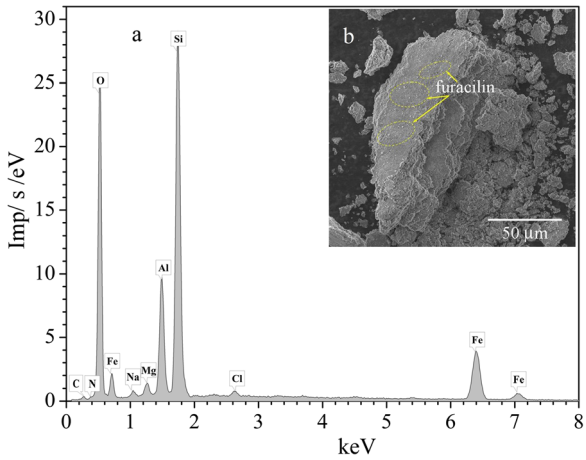

Fig. 8 EDX analysis (**a**) and SEM image (**b**) of the bentonite/magnetite composite after nitrofurazone adsorption

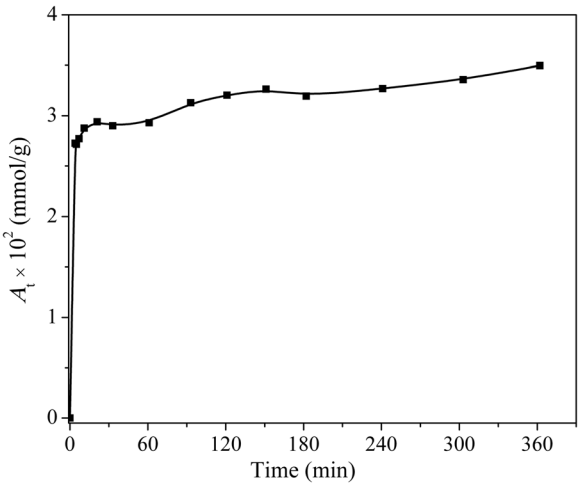

Fig. 10 Effect of contact time with regard to nitrofurazone adsorption onto bentonite/magnetite composite (pH = 5.5; adsorbent dosage = 1 g/L; $C_0 = 6.813\times10^{-2}$ mmol/L)

bentonite/magnetite particles were aggregated with various morphologies and sizes <50 μm (Fig. 7). This result agreed well with the granulometric analysis (Fig. 3b). Elemental analysis for O, Si, Al, and Mg estimated their contents to be 28.9, 20.3, 7.5, and 1.0 wt.%, respectively. Iron from magnetite accounted for 23.3 wt.% of the total composition of the composite. The analysis also identified chlorine and sulfur in the sample, which may have originated from the use of a solution containing $FeCl_3$ and $FeSO_4$.

The SEM image of the bentonite/magnetite surface after nitrofurazone adsorption (Fig. 8) showed changes during adsorption: namely, nitrofurazone was located on the surfaces of swollen clay particles. The presence of C and N was attributed to the nitrofurazone.

IR Spectroscopy Interactions between nitrofurazone and bentonite/magnetite were followed by FTIR spectroscopy. Peaks in the range 3700–3000 cm^{-1} from the composite were due to stretching bands for structural O–H and H–O–H from adsorbed water (Fig. 9, spectrum a). The band at 1635 cm^{-1} belongs to the deformation vibration of adsorbed H_2O molecules. The absorption band at 1400 cm^{-1} is assigned to the deformation vibrations of the OH groups at the edges of the Si–O tetrahedra. The band with a peak at 1042 cm^{-1} corresponds to the Si–O–Si valence vibrations of the SiO_4 tetrahedra in the Mnt. Fluctuations of the Si–O–Si rings in the SiO_4 tetrahedra and lattice vibration of Fe–O bonds in magnetite manifest themselves in the range 700–450 cm^{-1} (Ma et al. 2003; Khashirova et al. 2009; Lou et al. 2015).

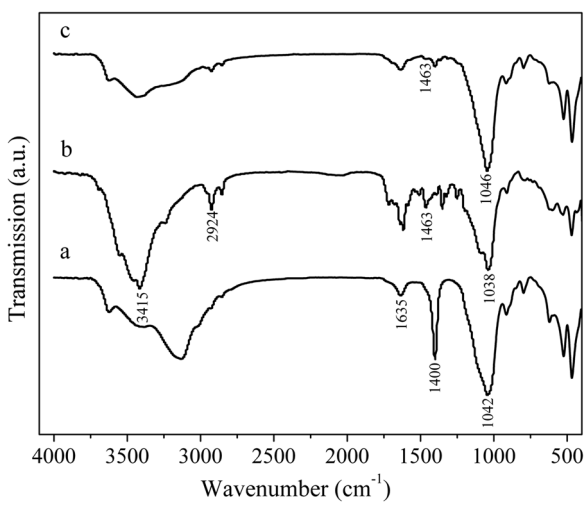

Fig. 9 IR spectra of (**a**) bentonite/magnetite composite, (**b**) nitrofurazone, and (**c**) bentonite/magnetite composite after nitrofurazone adsorption

In the nitrofurazone spectrum (Fig. 9, spectrum b), a broad absorption band was observed in the region of 3700–3000 cm^{-1}. A maximum at 3415 cm^{-1} corresponds to the N–H stretching vibrations in the amide group. The absorption band at 2924 cm^{-1} is assigned to the stretching vibrations of the CH_3 group. The absorption bands in the region 1700–1500 cm^{-1} correspond to the stretching vibrations of the C=O, C=C, C–NO_2 groups, and to deformation vibrations of the NH group. The absorption band at 1463 cm^{-1} is assigned to the deformation vibrations of the CH group in the furfural ring. The intense absorption band with a maximum at 1038 cm^{-1} corresponds to the deformation vibrations of the C–O–C group.

In the spectrum of bentonite/magnetite composite after adsorption of nitrofurazone (Fig. 9, spectrum c), a significant change in the contour of the absorption band in the region 3700–2900 cm^{-1} and an increase in its half width were observed. These changes are believed to be caused by rearrangements in the hydrogen bond system of the adsorbent. The absorption band at 1046 cm^{-1} shifted by 4 cm^{-1} toward a higher wavenumber. The presence of nitrofurazone in the sorbent was confirmed by the low-intensity absorption band at 1463 cm^{-1}.

https://doi.org/10.1007/s42860-019-00037-w Published online by Cambridge University Press

Table 5 Kinetics parameters of nitrofurazone adsorption by the magnetized bentonite/magnetite composite

Model	R^2	$\chi^2_{red}\times10^4$, $\left[\frac{mmol}{g}\right]^2$	$A_{eq}\times10^2$, $\frac{mmol}{g}$	k_1 (min^{-1})	k_2, $\frac{g}{mmol\times min}$
I	0.949	0.037	3.136	0.423	-
II	0.972	0.021	3.212	-	32.251

The totality of changes identified in the spectrum of bentonite/magnetite after nitrofurazone adsorption suggests that nitrofurazone adsorption was accompanied by the formation of hydrogen bonds between the NH groups in nitrofurazone and oxygen-containing groups in bentonite.

Kinetics The kinetics curve characterizing the accumulation of the drug in the adsorbent phase shows that the A_t value increased very quickly and reached the limit (Fig. 10). This was caused by the strong driving force of the concentration gradient at the beginning of the process due to the numerous adsorption sites available. The adsorption level reached 65% after 6 h.

The adsorption kinetics for the adsorbent/nitrofurazone system were analyzed using the models of both pseudo-first-order (Eq. 2, model I) and pseudo-second-order (Eq. 3, model II).

The greater R^2 value and the smaller χ^2_{red} for model II compared to model I (Table 5) led to the conclusion that nitrofurazone adsorption by bentonite/magnetite powder is better described by kinetics model II. The goodness of fit of the pseudo-second order kinetics indicates that chemical rather than physical adsorption controls the rate of nitrofurazone adsorption.

The nitrofurazone adsorption was also modeled according to the Langmuir, Freundlich, and Temkin isotherms, given by Eqs. 5, 6, and 7, respectively. In the equilibrium solution concentration range of 0 to ~0.05 mmol/L, the amount of nitrofurazone in the sorbed phase increased almost linearly (Fig. 11), indicating that adsorption depended only on the amount of drug transported to the adsorbent surface and the number of adsorption sites was not limiting. However, at higher equilibrium solution concentrations, the isotherm became curvilinear due to a limited number of available adsorption sites.

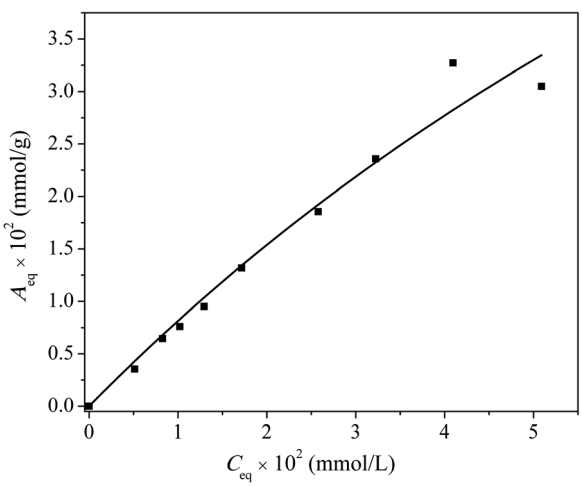

Fig. 11 Adsorption isotherm of nitrofurazone onto bentonite/magnetite composite (pH = 5.5; adsorbent dosage = 1 g/L)

Comparing the constants derived from these models, as well as comparing values for R^2 and χ^2_{red} (Table 6), revealed that the adsorption of nitrofurazone on bentonite/magnetite was described less well by the Temkin isotherm (lower R^2 and greater χ^2_{red}) and best by the Langmuir and Freundlich models, which differed little in their ability to predict the experimental results.

Apparently, with a further increase in nitrofurazone concentration in solution, the A_{eq} value increased and reached the limiting magnitude due to the deficiency of adsorption sites on the adsorbent surface. However, this cannot be tested experimentally because greater concentrations are beyond the range of the calibration curve and, thus, the accuracy of the method is compromised (Fig. 2).

The magnetic character of the bentonite/magnetite system (see above) was undiminished by nitrofurazone adsorption, so this is an effective system for removing the drug from the liquid medium under an external magnetic field (Fig. 12).

CONCLUSIONS

In the present study, bentonite/magnetite powder was pro-

Table 6 Constants and the adequacy indicators derived from adsorption models of nitrofurazone on the bentonite/magnetite composite

Model	Model parameters	Value
Langmuir	A_m (mmol/g)	0.139
	K_L (L/mmol)	6.204
	R^2	0.973
	$\chi^2_{red}\times10^4$ $(mmol/g)^2$	0.039
Freundlich	$1/n$	0.880
	K_F $\left(\frac{mmol^{1-1/n}L^{1/n}}{g}\right)$	0.468
	R^2	0.961
	$\chi^2_{red}\times10^4$ $(mmol/g)^2$	0.052
Temkin	$B_T\times10^2$ (mmol/g)	1.328
	$K_T\times10^{-2}$ (L/mmol)	1.015
	R^2	0.928
	$\chi^2_{red}\times10^4$ $(mmol/g)^2$	0.094

https://doi.org/10.1007/s42860-019-00037-w Published online by Cambridge University Press

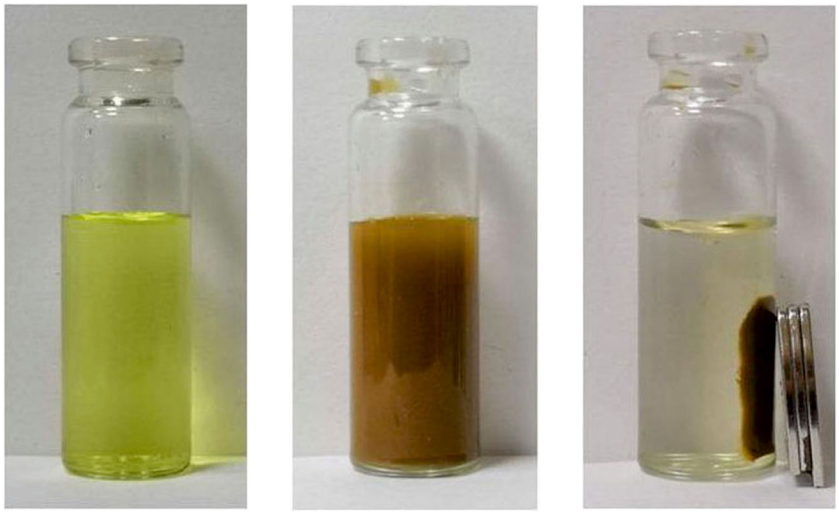

Fig. 12 Photographs illustrating the removal of nitrofurazone using a magnetic field

duced by co-precipitation of iron salts onto or into the clay layers and was characterized using a variety of methods. Based on the data of both laser diffraction and scanning electron microscopy, the particle size produced was <50 μm. X-ray diffraction analysis showed that the Fe_3O_4 phases were unchanged upon incorporation into the bentonite/magnetite composite; magnetization curves confirmed that the bentonite/magnetite particles were ferromagnetic. The bentonite/magnetite composite had a significant adsorption capacity for nitrofurazone, giving a value of 3.2×10^{-2} mmol/g of composite. The adsorption level reached 65% after 6 h. The adsorption kinetics were well described by a pseudo-second-order mechanism. These findings suggest that bentonite/magnetite materials can serve as magnetic adsorbents for removing pharmaceutical compounds from contaminated water bodies.

ACKNOWLEDGMENTS

The work was supported by the Russia Foundation for Basic Research (Grant N 18-43-370015-a). Measurements were performed in the centre for joint use of scientific equipment "The Upper Volga Region Centre of Physicochemical Research."

Compliance with Ethical Standards

Conflicts of Interest

On behalf of all authors, the corresponding author states that there is no conflict of interest.

REFERENCES

Abidi, N., Duplay, J., Jada, A., Errais, E., Ghazi, M., Semhi, K., & Trabelsi-Ayadi, M. (2019). Removal of anionic dye from textile industries' effluents by using Tunisian clays as adsorbents. Zeta potential and streaming-induced potential measurements. *Comptes Rendus Chimie, 22*, 113–125.

Alekseeva, O. V., Rodionova, A. N., Bagrovskaya, N. A., Agafonov, A. V., & Noskov, A. V. (2017). Effect of the organobentonite filler on structure and properties of composites based on hydroxyethyl cellulose. *Journal of Chemistry, 2017*, 1603937.

Alekseeva, O. V., Rodionova, A. N., Bagrovskaya, N. A., Agafonov, A. V., & Noskov, A. V. (2019). Effect of the bentonite filler on structure and properties of composites based on hydroxyethyl cellulose. *Arabian Journal of Chemistry, 12*, 398–404.

ALOthman, Z. A. (2012). A review: Fundamental aspects of silicate mesoporous materials. *Materials, 5*, 2874–2902.

Barraqué, F., Montes, M. L., Fernández, M. A., Mercader, R. C., Candal, R. J., & Sánchez, R. M. T. (2018). Synthesis and characterization of magnetic-montmorillonite and magneticorgano-montmorillonite: Surface sites involved on cobalt sorption. *Journal of Magnetism and Magnetic Materials, 466*, 376–384.

Bee, S.-L., Abdullah, M. A. A., Bee, S.-T., Sin, L. T., & Rahmat, A. R. (2018). Polymer nanocomposites based on silylated-montmorillonite: A review. *Progress in Polymer Science, 85*, 57–82.

Biosic, M., Skoric, I., Beganovic, J., & Babic, S. (2017). Nitrofurantoin hydrolytic degradation in the environment. *Chemosphere, 186*, 660–668.

Cazetta, A. L., Vargas, A. M. M., Nogami, E. M., Kunita, M. H., Guilherme, M. R., Martins, A. C., Silva, T. L., Moraes, J. C. G., & Almeida, V. C. (2011). NaOH-activated carbon of high surface area produced from coconut shell: Kinetics and equilibrium studies from the methylene blue adsorption. *Chemical Engineering Journal, 174*, 117–125.

Datta, S. M. (2013). Clay–polymer nanocomposites as a novel drug carrier: Synthesis, characterization and controlled release study of Propranolol Hydrochloride. *Applied Clay Science, 80–81*, 85–92.

Deng, L., Yuan, P., Liu, D., Annabi-Bergaya, F., Zhou, J., Chen, F., & Liu, Z. (2017). Effects of microstructure of clay minerals, montmorillonite, kaolinite and halloysite, on their benzene adsorption behaviors. *Applied Clay Science, 143*, 184–191.

Dordio, A. V., Miranda, S., Ramalho, J. P. P., & Carvalho, A. J. P. (2017). Mechanisms of removal of three widespread

pharmaceuticals by two clay materials. *Journal of Hazardous Materials, 323*(Part A), 575–583.

Gamba, M., Kovář, P., Pospíšil, M., & Sánchez, R. M. T. (2017). Insight into thiabendazole interaction with montmorillonite and organically modified montmorillonites. *Applied Clay Science, 137*, 59–68.

Gil, A., Korili, S. A., & Vicente, M. A. (2008). Recent advances in the control and characterization of the porous structure of pillared clay catalysts. *Catalysis Reviews, 50*, 153–221.

Golubeva, O. Y. (2016). Effect of synthesis conditions on hydrothermal crystallization, textural characteristics and morphology of aluminum-magnesium montmorillonite. *Microporous and Mesoporous Materials, 224*, 271–276.

Grenni, P., Ancona, V., & Caracciolo, A. B. (2018). Ecological effects of antibiotics on natural ecosystems: A review. *Microchemical Journal, 136*, 25–39.

Ho, Y.-S. (2004). Citation review of Lagergren kinetic rate equation on adsorption reactions. *Scientometrics, 59*, 171–177.

Jaynes, W. F., & Boyd, S. A. (1991). Clay mineral type and organic compound sorption by hexadecyltrimethlyammonium-exchanged clays. *Soil Science Society of America Journal, 55*, 43–48.

Khashirova, S. Y., Musaev, Y., Mikitaev, A. K., Malkanduev, Y. A., & Ligidov, M. K. (2009). Hybrid nanocomposites based on guanidine methacrylate monomer and polymer and layered aluminosilicates: Synthesis, structure and properties. *Polymer Science. Series B, 51*, 377–382.

Lee, C. H., Kato, M., & Usuki, A. (2011). Preparation and properties of bio-based polycarbonate/clay nanocomposites. *Journal of Materials Chemistry, 21*, 6844–6847.

Liao, M. H., & Chen, D. H. (2002). Preparation and characterization of a novel magnetic nano-adsorbent. *Journal of Materials Chemistry, 12*, 3654–3659.

Lin, S., Zhou, T., & Yin, S. (2017). Properties of thermally treated granular montmorillonite-palygorskite adsorbent (GMPA) and use to remove Pb^{2+} and Cu^{2+} from aqueous solutions. *Clays and Clay Minerals, 65*, 184–192.

Lou, Z., Zhou, Z., Zhang, W., Zhang, X., Hu, X., Liu, P., & Zhang, H. (2015). Magnetized bentonite by Fe_3O_4 nanoparticles treated as adsorbent for methylene blue removal from aqueous solution: Synthesis, characterization, mechanism, kinetics and regeneration. *Journal of the Taiwan Institute of Chemical Engineers, 49*, 199–205.

Ma, M., Zhang, Y., Yu, W., Shen, H., Zhang, H., & Gu, N. (2003). Preparation and characterization of magnetite nanoparticles coated by amino silane. *Colloids and Surfaces A: Physicochemical and Engineering Aspects, 212*, 219–226.

Martinez-Costa, J. I., Leyva-Ramos, R., & Padilla-Ortega, E. (2018). Sorption of diclofenac from aqueous solution on an organobentonite and adsorption of cadmium on organobentonite saturated with diclofenac. *Clays and Clay Minerals, 66*, 515–528.

Park, K. W., Jung, J. H., Kim, J. D., Kim, S. K., & Kwon, O. Y. (2009). Preparation of mesoporous silica-pillared H^+-titanosilicates. *Microporous and Mesoporous Materials, 118*, 100–105.

Pastukhov, A. V., Davankov, V. A., Lubentsova, K. I., Kosandrovich, E. G., & Soldatov, V. S. (2013). Structure and properties of magnetic composite sorbents based on hypercrosslinked polystyrenes. *Russian Journal of Physical Chemistry A, 87*, 1702–1708.

Ruiz-Hitzky, E., Aranda, P., Dardera, M., & Rytwo, G. (2010). Hybrid materials based on clays for environmental and biomedical applications. *Journal of Materials Chemistry, 20*, 9306–9321.

Sahnoun, S., Boutahala, M., Tiar, C., & Kahoul, A. (2018). Adsorption of tartrazine from an aqueous solution by octadecyltrimethylammonium bromide-modified bentonite: Kinetics and isotherm modeling. *Comptes Rendus Chimie, 21*, 391–398.

Sebayang, P., Kurniawan, C., Aryanto, D., Setiadi, E. A., Tamba, K., Djuhana, & Sudiro, T. (2018). Preparation of Fe_3O_4/bentonite nanocomposite from natural iron sand by co-precipitation method for adsorbents materials. *IOP Conference Series: Materials Science and Engineering, 316*, 012053.

Yu, W. H., Li, N., Tong, D. S., Zhou, C. H., Lin, C. X., & Xu, C. Y. (2013). Adsorption of proteins and nucleic acids on clay minerals and their interactions: A review. *Applied Clay Science, 80–81*, 443–452.

Zhang, W. H., Ding, Y. J., Boyd, S. A., Teppen, B. J., & Li, H. (2010). Sorption and desorption of carbamazepine from water by smectite clays. *Chemosphere, 81*, 954–960.

Zhou, C. H., Shen, Z. F., Liu, L. H., & Liu, S. M. (2011). Preparation and functionality of clay-containing films. *Journal of Materials Chemistry, 21*, 15132–15153.

(*Received 14 May 2019; revised 4 October 2019; AE: William F. Jaynes*)